Ordered Structure in Blends of Block Copolymers. 5. Blends of Lamella-Forming Block Copolymers Showing both Microphase Separation Involving Unique Morphological Transitions and Macrophase Separation†

Daisuke Yamaguchi, Shuntaro Shiratake,‡ and Takeji Hashimoto*

Department of Polymer Chemistry,Graduate School of Engineering, Kyoto University, Kyoto 606-8501, Japan

Received May 15, 2000; Revised Manuscript Received September 5, 2000

ABSTRACT: It is pointed out theoretically that the ordered morphology in the binary mixtures of A−B type diblock copolymers, ((A−B)$_1$/(A−B)$_2$), depends not only on the compositions of block copolymers (i.e., the volume fraction of the A block, f_{A1}, f_{A2}) but also on the relative chain-length differences of the constituent copolymers (α_j for jth (j = A or B) block where α_j is defined by $\alpha_j = (N_j^2 - N_j^1)/N_j^1$ and N_j^i (i = 1 or 2) denotes the polymerization index of the jth block chain in the ith block copolymer (A−B)$_i$) and blend composition (i.e., the mole fraction of (A−B)$_2$ having a larger molecular weight, q_2), whereas the morphology in the single component A−B diblock copolymer system in a strong segregation limit solely depends on the composition (f_A). We explored ordered morphology of binary mixtures of lamella-forming polystyrene (PS)-*block*-polyisoprene (PI), (PS−PI), with given block compositions ($f_{PS1} = 0.44$, $f_{PS2} = 0.46$) and given relative chain-length differences ($\alpha_{PS} = 6.18$, $\alpha_{PI} = 5.68$) as a function of q_2. Our results revealed both the regime where only microphase separation occurred ($q_2 = 0$ and $0.179 \le q_2 \le 1$) and the regime where macrophase separation occurred as well ($0.003 \le q_2 \le 0.127$). In the microphase separation regime, we found a unique morphological transition between lamellar and cylindrical morphology with q_2 whose trend is consistent with the theoretical prediction by Lyatskaya et al. (*Polymer* **1992**, *33,* 343). In the macrophase separation regime we found the two coexisting macrophases with cylindrical and lamellar morphology. The miscibility gap of the two PS−PIs, with respect to q_2 for the macrophase separation, was found to be consistent with a theoretical prediction by Matsen (*J. Chem. Phys.* **1995**, *103,* 3268).

I. Introduction

Diblock copolymers have received considerable experimental and theoretical attention, due to their interesting and potentially useful properties and structures, such as the order−disorder transition (ODT) and the wide varieties of morphologies in the ordered state.[1,2] Recently blends of A−B diblock copolymers, the type of (A−B)$_\alpha$/(A−B)$_\beta$, have also received much experimental[3−11] and theoretical attention,[12−17] because they show a broad array of interesting behavior, including macrophase separation,[5] microphase separation,[3,4,11] macrophase separation induced by microphase separation,[6,7] order−order transitions,[8−10] and modulated or superlattice structures.[7]

Throughout the previous studies of this series,[5−7,11] we have consistently paid our attention to the phenomena peculiar to the binary blends of A−B diblock copolymers. In parts 1−3 of this series,[5−7] we explored the miscibility criterion and the detail of the complex morphology resulted from the macrophase separation of the constituent copolymers in binary mixtures of polystyrene(PS)-*block*-polyisoprene(PI) copolymers (PS−PI), where the two constituent copolymers have nearly same compositions but different molecular weights. They have either symmetric[5,6] or asymmetric compositions.[7] Then in part 4 of this series,[11] we found an unusual behavior of domain spacing with temperature in binary mixtures of PS−PI copolymers with different compositions and molecular weights in the criterion where the two copolymers are miscible. Namely, in the case of neat PS−PI copolymers their domain spacing always increase with decreasing temperature,[18] whereas the domain spacing of a binary blend of PS−PI copolymers investigated in ref 11 decreased with decreasing temperature. We elucidated that this unusual behavior is due to delocalization of chemical junctions of the short diblock copolymers from the interface between the PS and PI lamellae with temperature by the combination of small-angle X-ray scattering (SAXS) and neutron scattering (SANS) methods.

In this paper, we will report two unique features found for binary blends of nearly symmetric and lamella-forming PS−PI copolymers upon varying blend compositions: (i) a unique morphological transition in microphase separation regime and (ii) macrophase separation.

When we focus on the binary blends of A−B diblock copolymers in which both copolymers have similar compositions but different molecular weights, we see that several studies have dealt with the blends of compositionally symmetric diblock copolymers.[5,19−22] In the first of this series of papers,[5] we examined the miscibility criterion for several pairs of PS−PI copolymers whose copolymer composition, f_{PS} (volume fraction of polystyrene), covered 0.35−0.69. The conclusion is that in the case where the molecular weight ratio of two PS−PI copolymers was smaller than 5, they were totally miscible, while in the case where the molecular weight

* To whom correspondence should be addressed.

† Presented in part at the 46th Symposium of the Society of Polymer Science, Japan, Oct., 1997. *Polym. Prepr. Jpn., Soc. Polym. Sci., Jpn.* **1997**, 46, 2649−2650.

‡ Present address: Nissho Iwai Co., Ltd. 4-5, Akasaka 2-chome, Minato-ku, Tokyo 107-8655, Japan

10.1021/ma000827d CCC: $19.00
Published on Web 10/14/2000

ratio was greater than 10, the two constituent copolymers showed partial miscibility and macroscopically phase-separated structures, depending on the blend composition. This result has good agreement with theoretical work[16] and other experimental works.[19,21]

On the theoretical side, Matsen examined the miscibility of two A−B diblock copolymers both having symmetric composition but different total polymerization indices, using self-consistent field theory (SCFT).[16] His calculation predicts that when the molecular weight ratio exceeds about 5, they become immiscible and show macroscopically phase-separated structures.

Two experimental works on diblock blends, both having symmetric composition, one of which mainly examined miscible pairs of PS−PI diblock copolymer blends[19] and the other of which examined immiscible pairs of polystyrene (PS)-*block*-polybutadiene (PB) diblock copolymer blends,[21] show quite good agreements with the phase diagram of Matsen's theoretical work.[16]

Another interest in this type of blend (i.e., diblock blends, both having symmetric composition) is the possibility of the blends having a morphology other than lamellae, because the possibility cannot be ever either expected or found actually for single component diblock copolymers having corresponding block compositions. In ref 5, both SAXS profiles and TEM micrographs presented a new unidentified morphology for the blend of lamellar forming block copolymers with a particular blend composition, though a possible origin was not discussed in detail in that paper.

Lin et al.[20] obtained some interesting SAXS profiles in another kind of miscible pair of nearly symmetric PS−PI diblock copolymers, composed of one which has a lamellar morphology and another which has a disordered homogeneous state due to its considerably low molecular weight. However, they could not identify its morphology.

On the theoretical side, Lyatskaya et al.[23] predicted the possibility of the morphological transition from lamellar to cylinder in the binary blend of lamellar-forming (i.e., compositionally nearly symmetric) diblock copolymers. In their calculations, they used the strong-segregation theory (SST) instead of SCFT. Although the SST has a serious disadvantage in that it cannot predict the immiscibility of the two diblocks,[16,24] it can be quite valuable due to its simple formulation.

In this paper, we first present the experimental results of the binary blends of nearly symmetric, lamella-forming PS−PI diblock copolymers that undergo either no macrophase separation or a macrophase separation of the constituent copolymers, depending on the blending composition. For the systems with the blending compositions for which no macrophase separation occurred, we found a morphological transition from lamellar to cylinder with varying the blending composition. We have applied the SST formulation proposed by Lyatskaya et al.[23] to the system showing the morphological transition. We found that the theoretical prediction was consistent with the experimental result: the theory correctly predicts the decrease of the free energy of the cylinder phase relative to the lamellar phase at the experimentally relevant blend composition, though the theory fails to predict the cylinder phase to be stable. For the system with the blend compositions for which the macrophase separation occurred, we apply the SCFT theory by Matsen[16] to compare the experimental and theoretical miscibility criterion with respect to the blending composition.

Table 1. Sample Characteristics

code[a]	M_n	M_w/M_n	M_n(PS)[b]	M_n(PI)[c]	w_{PS}[d]
OSI-3	1.5×10^4	1.02	7.0×10^3	7.5×10^3	0.48
H102	1.0×10^5	1.16	5.0×10^4	5.0×10^4	0.50

[a] H102 and OSI-3 were the same samples used in refs 25 and 26, respectively. [b] M_n(PS) is the number-average molecular weight of the PS block. [c] M_n(PI) is the number-average molecular weight of the PI block. [d] w_{PS} is the weight fraction of PS block in the PS−PI diblock copolymer.

II. Experimental Section

Two nearly symmetric and lamellar-forming diblock copolymers of the type PS−PI used in this study were synthesized by living anionic polymerization with *sec*-butyllithium as an initiator and cyclohexane as a solvent. Characteristics of these copolymers are summarized in Table 1. Film specimens were cast from a toluene solution containing 5 wt % polymer, and then dried until a constant weight was attained. The film specimens were further annealed in order to achieve a near-equilibrium state at 150 °C, which is above the glass transition temperature of the PS (∼100 °C), under nitrogen atmosphere for 4 h. Although a variety of blend specimens with different compositions were prepared and investigated in this study, whose results will be summarized in Table 4 or Figure 8 later, our attention is focused mainly on the three blend specimens designated as 20/80, 60/40, and 70/30, representing the weight ratio of the long diblock (H102) to the short diblock (OSI-3).

Small-angle X-ray scattering, SAXS, was measured on the film specimens with a SAXS apparatus described elsewhere, except, in some cases, for the replacement of the X-ray generator with a new one (MAC Sciences M18X HF operated at 18 kW).[27−29] SAXS profiles were obtained with a one-dimensional position-sensitive proportional counter (PSPC) and corrected for air scattering, absorption, and thermal diffuse scattering[27−29] but were not desmeared. All measurements were conducted with specimens placed with the "edge configuration". Namely, the film specimens with 0.5 mm thickness were cut off into rectangles with 15 mm length and 3 mm width, stacked up along the film normals to the total thickness of 3 mm, and placed with their film normals parallel to the one-dimensional PSPC. The incident X-ray beam comes to the sample along the direction perpendicular to the film normals and parallel to the film width. A further description is given in Figure 1 of ref 25b.

For transmission electron microscopy (TEM), the film specimens were microtomed at −100 °C, using a Reichert Ultracut E low-temperature sectioning system. The ultrathin sections were stained with the vapor of 2% OsO_4(aq) for a few hours. Electron microscope observation was done with a Hitachi H-600 transmission electron microscope operated at 75 kV.

III. Results

A. SAXS Results. In Figure 1, we show the SAXS profiles for each of the blends (b−d) as well as for the two pure diblock copolymers (a and e). The logarithm of the SAXS intensity is plotted against the magnitude of scattering vector, q, defined by $q = (4\pi/\lambda)\sin(\theta/2)$ where λ and θ are the wavelength of the incident X-ray and the scattering angle, respectively. In all cases we observe scattering profiles showing higher-order scattering peaks.

For the pure long diblock (a) 100/0, we observe nine scattering peaks as marked by arrows. The higher-order peaks which are located at the positions of integer multiples of the first-order scattering peak position indicate that alternating lamellar microdomains of PS

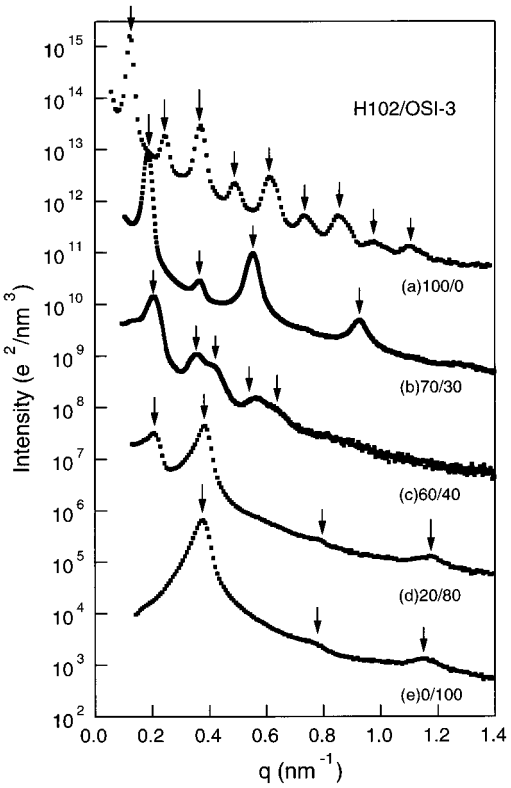

Figure 1. SAXS profiles obtained for the binary blends of H102/OSI-3 with compositions of (a) 100/0 (wt %/wt %), (b) 70/30, (c) 60/40, (d) 20/80, and (e) 0/100. The scattering peaks in each profile are marked by arrows.

and PI were formed, as expected from a nearly symmetric volume fraction.[30]

For the pure short diblock (e) 0/100 and (b) 70/30 blend as well, we can, respectively, identify two and three higher-order scattering peaks whose positions are integer multiples of the first-order scattering peak position, as marked by arrows, and hence anticipate lamellar morphology. Note that a very weak second-order scattering peak and a lack of the fourth-order scattering maximum in the SAXS profile of the 70/30 blend (b) are due to approximately equal volume fractions of PS and PI domains, and a relatively weak third-order scattering peak in the SAXS profile of neat short block copolymer ((e) 0/100) is due to lattice distortion of lamellar microdomains in the weak-segregation regime inherent to relatively low molecular weight diblock copolymers.[31−34]

For (c) the 60/40 blend, the SAXS profile clearly showed four higher-order scattering peaks at positions of $\sqrt{3}$, $\sqrt{4}$, $\sqrt{7}$, and $\sqrt{9}$ relative to the position of the first-order peak, which are due to hexagonally packed cylindrical morphology. Thus, the morphological transition from lamellar to cylinder seems to occur between 70/30 blend and 60/40 blend with varying the blend composition of the two **lamella-forming** block copolymers.

For (d) the 20/80 blend, the second-order peak intensity is larger than the first-order peak intensity. If we assume that this scattering profile was obtained from a single morphology, the shape of profile is very unusual. Another possibility is that this scattering profile is a superposition of two different scattering profiles[5,7,35] that reflect two coexisting phases in the 20/80 blend, as will be described immediately below.

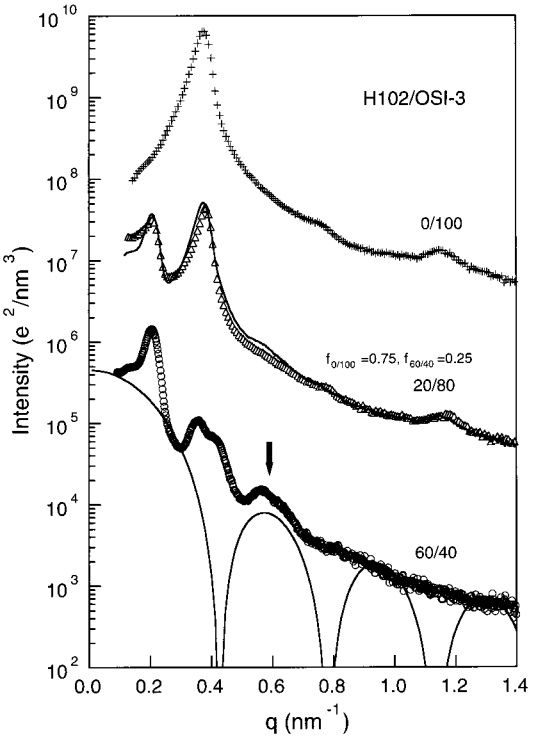

Figure 2. Comparison of scattering profiles for H102/OSI-3 = 20/80 blend (△) with a best-fit calculated profile (solid line). The calculated profile is obtained by averaging the SAXS profile from neat OSI-3 (+) and that from a 60/40 blend of H102/OSI-3 (○), with a weighting factor of 0.75 for OSI-3 and 0.25 for the 60/40 blend. The bottom solid line is the calculated curve for the cylinder form factor having sharp interface with the radius of R = 9.0 nm and the first-order maximum as indicated with a thick arrow.

In Figure 2, we show three SAXS profiles for the pure short diblock (0/100), 20/80 blend, and 60/40 blend in order to highlight that the profile for 20/80 is almost identical to a weighted average of the other two profiles for the 0/100 and 60/40 blends. The intuition that the weighted average of the profiles of the pure short diblock and 60/40 blend will give the profile for the 20/80 blend was obtained from a good coincidence of the peak positions (i.e., the first- and second-order scattering peaks in the 20/80 blend correspond to the first-order scattering peaks of the 60/40 blend and the neat short diblock (0/100), respectively). In addition, we have another piece of evidence supporting that the 20/80 blend forms two-coexisting microdomain morphologies, one corresponding to that of the 60/40 blend and the other to that of neat short diblock, respectively, as described later in section III.B. The solid line on the SAXS profile of 20/80 blend is a calculated curve, $I_{calc}(q)$, based on the following equation

$$I_{calc}(q) = f_{0/100}I_{0/100}(q) + f_{60/40}I_{60/40}(q) \qquad (1)$$

where $f_{0/100}$ and $f_{60/40}$ are the fraction of scattering profiles $I_{0/100}(q)$ and $I_{60/40}(q)$, respectively, with $f_{0/100} + f_{60/40} = 1$. The curves $I_{0/100}$ and $I_{60/40}$ are the SAXS profiles of the neat short diblock (0/100) and the 60/40 blend, respectively, as shown in Figure 2. The calculated profile obtained for $f_{0/100} = 0.75$ (and $f_{60/40} = 0.25$) was found to be best fitted to the measured profile of the 20/80 blend.

Note that if we assume that the 20/80 blend is composed of coexisting two kinds of ordered-micro-

domain phases, one of which is a lamellar phase corresponding to the pure short diblock and the other of which is a cylindrical phase corresponding to the 60/40 blend, the volume fractions of each phase (lamellar or cylindrical phase) are calculated to be 0.67 and 0.33, respectively, based on stoichiometric considerations. These values (0.67 and 0.33) are different from the volume fractions of the short diblock (0/100) and 60/40 blend components in the 20/80 blend, as estimated from SAXS measurement (i.e., $f_{0/100} = 0.75$ and $f_{60/40} = 0.25$). Therefore, the SAXS result seems to reflect the volume fractions of the two coexisting phases not completely correctly but somewhat biased toward the lamellar phase composed of a short diblock.

A discrepancy between measured and calculated profiles of the 20/80 blend exists in the range $0.5\ \text{nm}^{-1} \le q \le 0.65\ \text{nm}^{-1}$; that is, a broad and small shoulder in the calculated curve is slightly more remarkable than that in the measured scattering profile. This small shoulder in the calculated curve arises from the fourth- and fifth-order peaks in the measured scattering profile of the 60/40 blend, and hence we may conclude that the cylindrical phase in the 20/80 blend has a smaller grain size, less long-range order or larger paracrystalline lattice distortion[34] than that in the 60/40 blend. This may partially account for the observed discrepancy between the volume fractions of the two phases calculated from the stoichiometry and the SAXS profile.

In Figure 2, a calculated form factor scattering curve for cylindrical domains (solid line) is also shown along with the SAXS profile of the 60/40 blend. The scattering formula for cylindrical particles[36] that we used in this study is given by

$$f(q) = 2A_e V \Delta\rho \frac{J_1(qR)}{qR} \tag{2}$$

where $f(q)$ is the structure amplitude for a cylindrical particle, A_e is the scattering amplitude from electron, $\Delta\rho$ is the difference in the electron density between cylinders and their medium, V is the volume of the cylinders, and R is the cylinder radius. The scattered intensity $I(q)$ is a square of $f(q)$.

$$I(q) = [f(q)]^2 \tag{3}$$

The logarithm of $I(q)$ is plotted against q in Figure 2, where R is determined from the total volume fraction of PS block chain in the 60/40 blend, as described below, and the value of $2A_eV\Delta\rho$, which is related to only the absolute value of $I(q)$, is chosen such that the intensity level of $I(q)$ is close to that of the SAXS profile of the 60/40 blend. Assuming hexagonally packed cylindrical morphology, the volume fraction of cylinders, Φ_{cyl}, is given by

$$\Phi_{cyl} = (2\pi/\sqrt{3})(R/d_{cyl})^2 \tag{4}$$

where d_{cyl} is the intercylinder distance and obtained from the position of the first-order peak of SAXS profile, q_m, by $d_{cyl} = 4\pi/(\sqrt{3}q_m)$. For the 60/40 blend, we assumed that PS block chains form hexagonally packed cylindrical microdomains and obtained $\Phi_{cyl} = 0.46$ and $d_{cyl} = 35.6$ nm, and then R is determined to be 9.0 nm.

Comparing the form factor scattering curve with the SAXS profile of 60/40 blend, we see that the position of the first-order maximum in the form factor curve (marked by a thick arrow) and those of the fourth- and fifth-order peaks in the SAXS profile of the 60/40 blend are exactly the same. Therefore, we were able to identify scattering maxima from the form factor clearly in the SAXS profile of the 60/40 blend and determine the average radius of the cylindrical domain.

B. TEM Results. In Figure 3, TEM micrographs of neat long and short diblock copolymers as well as those of their blends, 70/30 and 60/40, are shown. These TEM images seem to be in good agreement with SAXS results. The TEM image for (b) the 70/30 blend, as well as those for neat diblock copolymers (a) 100/0 and (d) 0/100, shows alternating lamellar morphology. Note that, in the micrograph of the neat short diblock ((d) 0/100), some parts do not show clear alternating lamellar microdomains but undulated lamellar.[37,38] This reflects the observation that the short diblock copolymer having a relatively low molecular weight has the ODT close to the glass transition temperature (T_g) of the PS block and that hence it may be vitrified in the weak segregation regime.

On the other hand, for (c) the 60/40 blend, a TEM image typical of cylindrical morphology was observed. We consider that this image corresponds to that obtained in the section on which the cylindrical axes orient nearly normal to it. In this image the bright part, the PS phase, unstained by OsO_4, forms cylindrical microdomains. Thus, we concluded from TEM observation and SAXS measurement that in the 60/40 blend the two constituent copolymers, H102 and OSI-3, are uniformly mixed and self-assembled to a single microdomain morphology of hexagonally packed PS cylinders in the matrix of PI. Note that the hexagonal packing is not very clear from this TEM image. However, the SAXS profile, which clearly shows the second-order peak at a position of $\sqrt{3}$ relative to the position of the first-order peak, suggests hexagonal packing.

In Figure 4, TEM micrographs of the 20/80 blend are shown. From part a of Figure 4, we observe that a grain, which is composed of the larger microdomains and indicative of an H102-rich phase, is isolated in the matrix of the other phase composed of nearly pure OSI-3. From an enlarged micrograph shown in part b of Figure 4, we can observe the microdomain morphologies of two coexisting phases. In the area composed of smaller microdomains, some parts show alternating lamellar morphology, the other parts show distorted lamellae or the disordered morphology, and they are almost identical with what we have observed in the pure short diblock copolymer (see part d of Figure 3). On the other hand the area composed of larger microdomains shows a morphology very similar to what we observed in the 60/40 blend (see part c of Figure 3). Such macrophase-separated morphologies were observed on each blend whose blend composition ranges between 2/98 and 50/50 (see Table 4 or Figure 8 later). In Figure 5, we show TEM images of (a) 2/98 and (b) 50/50 blends, which correspond to both ends of the composition range where macrophase separation occurred. By comparing Figure 5a and Figure 5b, we discern that indeed the volume fractions of H102-rich and OSI-3-rich phases are inverted, while the morphologies of these phases seem to be almost unchanged. Thus, we can conclude that, in the composition range between 2/98 and 50/50, H102 and OSI-3 phase-separate into two phases in which one phase consists of the nearly pure OSI-3 and the other phase consists of 60/40 wt %/wt % H102/OSI-3.

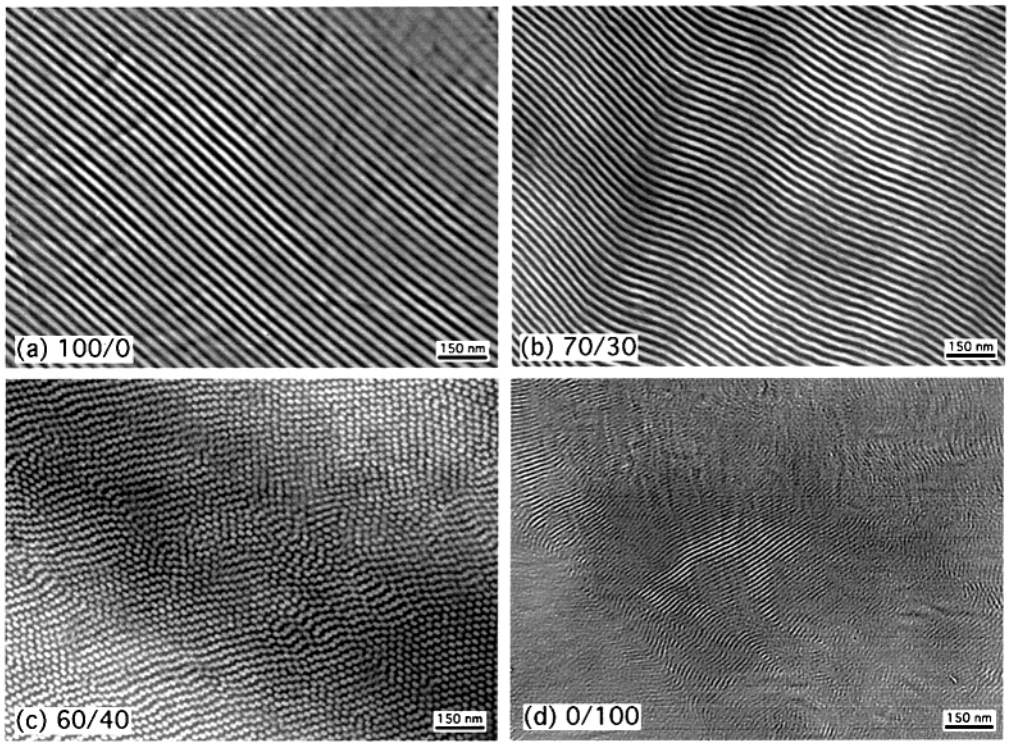

Figure 3. Transmission electron micrographs of the H102/OSI-3 binary mixtures with compositions (wt %/wt %) (a) 100/0, (b) 70/30, (c) 60/40, and (d) 0/100. Three of them, parts a, b, and d, show single-phase alternating lamellar morphology, and the other one, part c, shows single-phase morphology of hexagonally packed cylinders composed of polystyrene block chains in the matrix composed of polyisoprene block chains.

IV. Discussion

A. Morphological Transition from Lamellae to Cylinders with Blending Composition. In this section, we compare results predicted from the strong-segregation theory (SST) proposed by Lyatskaya et al.[23] with our experimental results about the morphological transition from lamellae to cylinders, which we have experimentally observed with changing blend composition of long (H102) and short (OSI-3) nearly symmetric lamella-forming diblock copolymers from 70/30 to 60/40 (shown in Figures 1 and 3).

Let us briefly describe the formulation of SST proposed by Lyatskaya et al.,[23] which hereafter we designate as the BZL model since the series of the papers[13,23,24,39,40] concerning this formulation were established by Birshtein, Zhulina, and Lyatskaya. In Figure 6, we schematically illustrate a binary mixture of A−B type diblock copolymers with large and small molecular weights which are self-assembled into (a) a lamellar microdomain or (b) a cylindrical microdomain without macrophase separation and with all their chemical junctions between A and B blocks localized at the interface. Here, the microdomain of each phase (i.e., A microdomain and B microdomain) is divided into two layers: (i) The layer designated as H_{j1} (where j = A or B) is composed of the whole j (j = A or B) chains of short diblock copolymers and some portions of j chains of long diblock copolymers. (ii) The layer designated as H_{j2} is composed of only the residual portion of j chains of long diblock copolymers. Each layer H_{ji} (i = 1, 2) has equal segmental density which is equal to segmental density of pure j polymer (j = A or B) (incompressibility). The incompressibility and the blend composition of the two block copolymers give relations between H_{j1} and H_{j2}.

Note that here all the j chains of long diblock copolymers are assumed to be divided into two nonoverlapping parts, one of which contains chemical junction points and resides in the H_{j1} layer, and the other of which contains chain ends and resides in the H_{j2} layer. This assumption is most fundamental and essential part of the SST.[13]

To examine the stable morphology for a blend of diblock copolymers, we consider the free energy per chain, ΔF, without taking into account the trivial contribution of the translational entropy of mixing.[23,24] Note that hereafter all the energetic values are expressed in kT units where k is the Boltzmann constant and T is absolute temperature. ΔF is given by

$$\Delta F = \Delta F_S + \Delta F_A + \Delta F_B \tag{5}$$

where ΔF_S is the surface free energy on the interface, and ΔF_A and ΔF_B are the conformational free energies, which are equivalent to the elastic free energies of A and B block chains in the microdomain space, respectively.

To calculate ΔF_S, ΔF_A, and ΔF_B we define the characteristic values of block copolymers that comprise the system as summarized in Table 2. According to ref 23, the shorter and longer diblock copolymers are designated as components 1 and 2, respectively, and the mixture composition is characterized by the number fraction (i.e., mol fraction), q_2, of component 2

$$q_2 = \frac{n_2}{n_1 + n_2} \tag{6}$$

where n_i are the number of molecules in each component. Note here that we define the fraction by q_2 instead of q in order to distinguish the quantity from the scattering vector q. Each component has A- and B-block chains. The polymerization index (i.e., number of mono-

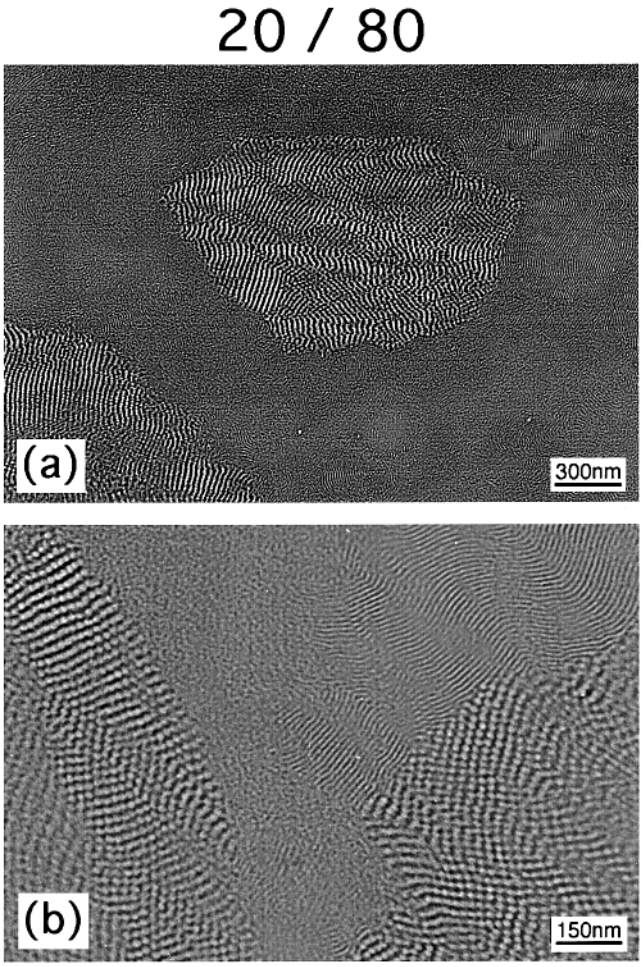

Figure 4. Transmission electron micrographs of the H102/OSI-3 = 20/80 (wt %/wt %) mixture taken at two different magnifications. The macrophase-separated structure between H102-rich phase and OSI-3-rich phase was observed.

mer units) of the j- (j = A or B) block chain of the *i*th component block copolymer $(A-B)_i$ (i = 1 or 2) is designated as N_j^i and

$$\alpha_j = \frac{N_j^2 - N_j^1}{N_j^1} (\geq 0) \tag{7}$$

is the relative difference between the lengths of j- (j = A or B) block chains of component 1 and 2. It is worthy to note that in order to specify the characteristic of two A−B block copolymers that compose the blend we need at least four independent parameters, and there is more than one way of choosing those four parameters. For example, to specify the total molecular weights of two constituent copolymers and their volume fractions of A blocks as four independent parameters is one way. However, in this paper we have chosen the polymerization indices of short block chains, N_A^1 and N_B^1, and the relative chain-length differences of the constituent copolymers, α_A and α_B, as four independent parameters due to consistency with ref 23.

Note that in this situation, the monomer volume, v, is assumed to be equal to both block chains for the simplicity and characterized by the unit length of a as $v = a^3$. Note further polymer stiffness of the jth block chain is characterized by the parameter $p_j = A_j/a$ where A_j is the Kuhn segment length of the jth polymer.

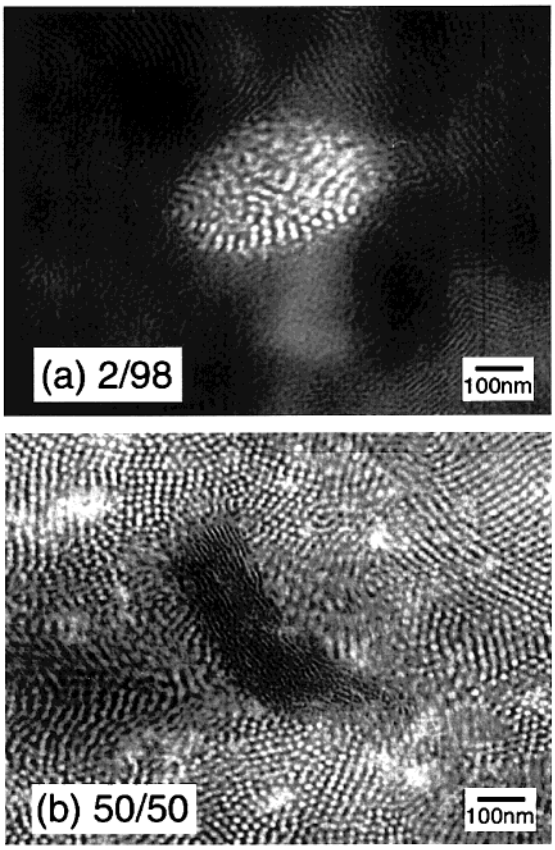

Figure 5. Transmisson electron micrographs of H102/OSI-3 blends with different compositions (wt %/wt %) (a) 2/98 and (b) 50/50. Both a and b show the macrophase separation of H102-rich and OSI-3-rich phases; however, the fractions of those phases are inverted.

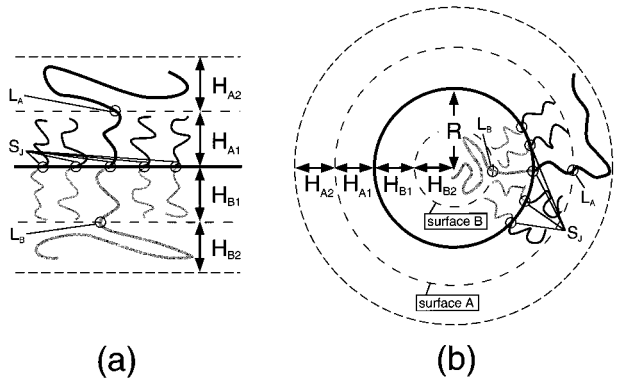

Figure 6. Schematic illustrations of (a) lamellar and (b) cylindrical morphology composed of binary mixture of AB diblock copolymers with similar compositions (both are nearly symmetric) but different chain lengths: H_{j1} (j = A or B) denotes the thickness of the sublayer where whole j chains of short diblock copolymer and some portion of j chains of long diblock copolymer reside, and H_{j2} denotes the thickness of the sublayer which is composed of only j chains of the long diblock copolymer.

Then for the surface free energy on the interface, we have

$$\Delta F_S = \frac{\Phi\sigma}{a^2} \tag{8}$$

where Φ/a^2 is the surface free energy coefficient (i.e., surface free energy per unit area, i.e., area/monomeric unit) of the interface and σ is the (average) interface area per block copolymer molecule.

Table 2. Characteristic Parameters for the BZL Model

	mol fraction	polymerizatoin index	
		A-block	B-block
component 1 (short diblock)	$1-q_2$	N_A^1	N_B^1
component 2 (long diblock)	q_2	$N_A^2 = (1+\alpha_A)N_A^1$	$N_B^2 = (1+\alpha_B)N_B^1$

For the elastic free energy, ΔF_j (j = A or B), according to the BZL model,[13,23,24,39] we can regard it as the sum of those of two layers, namely, H_{j1} and H_{j2}, presented in Figure 6

$$\Delta F_j = \frac{\sigma}{a^2}(\Delta F_{H_{j1}} + \Delta F_{H_{j2}}) \tag{9}$$

where $\Delta F_{H_{ji}}/a^2$ (j = A or B, and i = 1 or 2) refers to the elastic free energy of H_{ji} layer per unit area.

Here, at the beginning we consider the simplest case. Namely, both A and B domains consist of monodisperse block chains with the polymerization indices of $N^1_A(=N^2_A)$ and $N^1_B(=N^2_B)$, respectively, and they form a lamellar morphology. Moreover, for the sake of simplicity we assume here that the polymer stiffness is identical between A and B block chains, i.e., $p_A = p_B = p$ and $A_A = A_B = A$, as was done by the BZL formulation. Then, eq 9 is reduced to

$$\Delta F_j = \frac{\sigma}{a^2}\Delta F^{lam}_{H_{j1}} \tag{9'}$$

and, according to the BZL model,[13] $\Delta F^{lam}_{H_{j1}}$ is given by

$$\Delta F^{lam}_{H_{j1}} = \Delta F^{lam}_0(N^1_j,\sigma) = \frac{\pi^2}{8p}N^1_j\left(\frac{\sigma}{a^2}\right)^{-3} \tag{10}$$

Note that in eqs 9′ and 10 the superscript "lam" denotes planar interfaces and the subscript "0" denotes monodisperse chains. From eq 10, we see that the elastic free energy of one polymer chain (ΔF_{el}), which is composed of N^1_j monomers and confined in a tube with the base area of σ, is proportional to

$$\Delta F_{el} \propto \frac{N^1_j}{p}\left(\frac{\sigma}{a^2}\right)^{-2} \tag{11}$$

Equation 11 can be obtained from the free energy of a Gaussian chain whose end-to-end distance is H_{j1} (in kT units)[41]

$$\Delta F_{el} \propto \frac{(H_{j1})^2}{(N^1_j/p)A^2} \tag{12}$$

together with the condition of incompressibility.

$$\sigma H_{j1} = N^1_j a^3 \tag{13}$$

By substitution of the results of eqs 8, 9′, and 10 into eq 5, the free energy per molecule, ΔF, is written as a function of the only one independent parameter σ. Hence the equilibrium value of σ can be determined by the condition that ΔF is minimized, $d\Delta F/d\sigma = 0$. As a result of minimization, the equilibrium interface area, σ, as well as the half of the lamellar spacing, $H = H_{A1} + H_{B1}$, and the free energy per chain, ΔF, are given as follows:

$$\sigma = a^2\left(\frac{\pi^2}{4\Phi p}\right)^{1/3}N^{1/3} \tag{14}$$

$$H = a\left(\frac{4\Phi p}{\pi^2}\right)^{1/3}N^{2/3} \tag{15}$$

$$\Delta F = \frac{3}{2}\Phi\left(\frac{\pi^2}{4\Phi p}\right)^{1/3}N^{1/3} \tag{16}$$

where $N = N^1_A + N^1_B$ denotes the total polymerization index of the component 1. Note that eq 15 implies that the lamellar spacing is proportional to the two-thirds power of the copolymer's polymerization index. This relation has been experimentally confirmed.[42]

As for the binary mixture of the diblock copolymers, we can also obtain the equilibrium value of σ by the condition of $d\Delta F/d\sigma = 0$ for the both cases in which the mixture forms lamellar and cylindrical morphologies. In this case formulations of $\Delta F_{H_{j2}}$ in eq 9 are crucial and the resulting equations are rather complicated, in particular, for the case of cylindrical morphology. The thermodynamic advantage of the packing of chains with different lengths in such a way as depicted in Figure 6a or 6b is summarized as follows: In the region of H_{A2} and H_{B2}, the effective density of grafting (long) polymer chains, of which grafting points are designated as L_A and L_B in Figure 6, parts a and b, is basically reduced by a factor of q_2 in comparison with that in the region of H_{A1} and H_{B1} where the grafting (or junction) points are designated as S_J in Figure 6, parts a and b. Consequently $\Delta F_{H_{j2}}$ in eq 9 is considerably smaller than $\Delta F_{H_{j1}}$. The curvature of the interface affects the grafting density of the (long) polymer chains in the region of H_{A2} or H_{B2}, i.e., the density of L_A or L_B. In the case of planar interface (corresponding to Figure 6a), the effective area occupied per polymer chain is independent of the distance from the interface, namely, H_{A1} or H_{B1}, while in the case of surface A or surface B as defined in Figure 6b, the effective area occupied per polymer chain increases or decreases with the distance from the interface, i.e., H_{A1} or H_{B1}. Therefore, in the case of surface B, the lower density of L_B can be realized by suppressing the thickness of the H_{B1} layer. This suppression of the thickness H_{B1} forces the number of the segments of the long chain, which reside in the region of H_{B1}, to be less than N^1_B. On the other hand, in the case of a planar surface or surface A, the density of L_A is not reduced by suppressing H_{A1} and the number of the segments of the long chain, which reside in the region of H_{A1} is equal to N^1_A. In any case the surface densities of L_A and L_B are determined by minimizing the free energy of the systems.

Below we show only the resulting general expressions for σ_x, the interface area per chain, ΔF_x, the free energy per chain, and R_x, the characteristic domain size, corresponding to the half-width of B lamellae or the radius of the cylindrical domain, where x = C or L referring to cylinder or lamella, respectively. The details are available in the original papers.[13,23,24,39] However there are two different points between the following equations and the equations derived in the original paper,[23] due to our modifications. In eqs 15−20 of ref 23, the authors considered bimodal molecular weights only with respect to B-block chains ($N^1_B \neq N^2_B$) but

monodisperse molecular weight for A-block chains ($N_A^1 = N_A^2$), and equal stiffness between A- and B-block chains ($p_A = p_B$) for the sake of simplicity, whereas in this study we allow both A- and B-block chains to be bimodal and different stiffnesses ($p_A \neq p_B$) so as to apply the theory to our experimental situation.

$$\sigma_x = a^2(N_B^1)^{1/3}(PQ_x)^{1/3} \tag{17}$$

$$\Delta F_x = \frac{3}{2}\Phi(N_B^1)^{1/3}(PQ_x)^{1/3} \tag{18}$$

$$R_x = i_x(1 + \alpha_B q_2)N_B^1 a^3/\sigma_x = i_x a(1 + \alpha_B q_2)(N_B^1)^{2/3}(PQ_x)^{-1/3} \tag{19}$$

where $i_C = 2$, $i_L = 1$

$$P = \pi^2/4\Phi p_B \tag{20}$$

$$Q_C(q_2) = \frac{r^2}{2}G(\alpha_B,q_2) + \frac{p_B N_A^1}{p_A N_B^1}\frac{2(4 + 3h_{A1}/r)}{(2 + h_{A1}/r)^3} + \frac{p_B N_A^1}{p_A N_B^1}\alpha_A q_2^3\left(\frac{r}{r + h_{A1}}\right)^3\frac{2[4 + 3h_{A2}/(r + h_{A1})]}{[2 + h_{A2}/(r + h_{A1})]^3} \tag{21}$$

$$Q_L(q_2) = 1 + \alpha_B q_2^3 + \frac{p_B N_A^1}{p_A N_B^1}(1 + \alpha_A q_2^3) \tag{22}$$

In eq 21 r, h_{A1}, and h_{A2} are given by eqs 23−25, respectively

$$r = 2(1 + \alpha_B q_2) \tag{23}$$

$$\frac{h_{A1}}{r} = -1 + \sqrt{1 + \frac{N_A^1}{N_B^1}\left(\frac{1}{1 + \alpha_B q_2}\right)} \tag{24}$$

$$\frac{h_{A2}}{r} = \sqrt{1 + \frac{N_A^1}{N_B^1}\left(\frac{1 + \alpha_A q_2}{1 + \alpha_B q_2}\right)} - \sqrt{1 + \frac{N_A^1}{N_B^1}\left(\frac{1}{1 + \alpha_B q_2}\right)} \tag{25}$$

and the function $G(\alpha_B, q_2)$ is rather complicated as described below:

$$G(\alpha_B,q_2) = (1 + \alpha_B q_2)\{\sqrt{u^2 - l^2}[6u^2(1 + \alpha_B) + 0.5l^2u(1 - 5\alpha_B - 10\alpha_B^2) - 0.5l^2(1 + \alpha_B) - u^3(6 - \alpha_B - 5\alpha_B^2)] + [-0.5l^4\alpha_B(1 + 5\alpha_B) + 0.5l^2u^2(-10 + 3\alpha_B + 15\alpha_B^2) - 5u(u^2 - l^2)(1 + \alpha_B) + u^4(6 - \alpha_B - 5\alpha_B^2)]\} - 3l^2\alpha_B q_2 \tag{26}$$

Here l ($\equiv H_{B1}/R$, the ratio of the thickness of H_{B1} layer to the radius of the cylindrical domain, R) and u are determined by the following equations:

$$\frac{q_2}{1 + \alpha_B q_2} = \frac{\sqrt{1 - l^2(1 - \alpha_B^2)} - \alpha_B}{1 - \alpha_B^2} - l^2 \ln\frac{l(1 - \alpha_B)}{1 - \sqrt{1 - l^2(1 - \alpha_B^2)}} \tag{27}$$

$$u = \frac{1 - \alpha_B\sqrt{1 - l^2(1 - \alpha_B^2)}}{1 - \alpha_B^2} \tag{28}$$

Note that in the above expressions for cylindrical morphology the B-block chains are assumed to form cylinder domains and the A-block chains reside in the matrix phase as schematically depicted in Figure 5b. Equations 17−22 correspond to eqs 15−20 of ref 23 in the original formulation of the BZL model except for the difference noted earlier before eq 17. It should be mentioned here that ref 39, one of the original papers of the BZL model, contains two printing errors in eq 39. In this equation, one should replace u with u/r where u and r are defined by eq 31 of ref 39 and eq 32 of ref 39, respectively, and for the third term from the end of the right side, one should replace $-5(1 + \alpha)u^2(u^2 - l_1^2)$ with $-5(1 + \alpha)u(u^2 - l_1^2)$.[43] These corrections have been done in the calculation of this paper (see eqs 26 and 28 of this paper). In addition, as for the outside of the cylindrical domain (i.e., the matrix phase), the difference between the original BZL model[23,39] and this study is as follows: in the formulation of BZL model,[23,39] the free ends of block chains that form the convex layer against the B cylinder are assumed to be fixed at the external boundary (which is referred to as the FEF approximation[39]) and the elastic free energy of convex layers is calculated by eq 21 in ref 39, while in this paper we applied eq 18a in ref 39 to allow the probable distribution of the free ends of block chains instead of eq 21 in ref 39 for the calculation of free energy. However, as mentioned in ref 39, the difference between the values of free energy calculated by eqs 21 and 18a in ref 39 is expected to be small.

Now, let us apply expressions 17−22 to our experimental systems, H102/OSI-3 blends. The characteristic values of OSI-3 and H102, such as N_j^i, α_j, and p_j (j = PS or PI and i = OSI-3 or H102), which we used in the calculation, are summarized in Table 3, parts i and ii. Note that as for the degree of polymerization, we used the modified values, $\overline{N_j^i}$ (j = PS or PI and i = OSI-3 or H102), for which the asymmetry in segmental volume[44] is taken into account, instead of the intact values, N_j^i. $\overline{N_j^i}$ is given by

$$\overline{N_j^i} = (v_j/v_0)N_j^i \tag{29}$$

where $v_0 = (v_{PS}v_{PI})^{1/2}$ and we used the values of v_{PS} and v_{PI} as 107.2 and 81.9 cm^3/mol, respectively.[45,46] Note further that, to investigate the effect of the conformational asymmetry[47] on the morphologies, we have calculated the free energy in either case where the difference between p_{PS} and p_{PI} is taken into consideration or not. For the calculation, we have used the value of $\Phi p_{PS} = 0.5$ (in kT units) for the sake of convenience.[24]

In Figure 7, we plot the calculated value of $\Delta F_x/\Phi$ that is obtained from eq 18 as a function of q_2, the mol fraction of longer diblock component, namely H102. Note that here we used the reduced value of $\Delta F_x/\Phi$ for free energy to preclude evaluation of Φ. For Figure 7a, we did not take the conformational asymmetry between PS and PI into account; that is, $p_{PS} = p_{PI} = p$ and $\Phi p = 0.5$ are used in the calculation. However, for Figure 7b we took the conformational asymmetry into consideration; i.e., the values of p_j (j = PS or PI) in Table 3 and $\Phi p_{PS} = 0.5$ are used in the calculation.

Table 3

(i) Characteristics of Polymerization Indices of the PS and PI Blocks for the Two Block Copolymers OSI-3 and H102 Used for Calculations

i	N^{i}_{PS}[a]	N^{i}_{PI}[a]	$\bar{N}^{i}_{PS}$[b]	$\bar{N}^{i}_{PI}$[b]	f_{PS}[c]
OSI-3	67	110	76.7	96.1	0.44
H102	481	735	550.3	642.4	0.46

(ii) Relative Difference in the PS and PI Block Length α_j between the Two Block Copolymers OSI-3 and H102 and the Stiffness Parameter of PS and PI Block Chains p_j

j	α_j[d]	p_j[e]
PS	6.18	1.16
PI	5.68	1.26

[a] N^{i}_{PS} and N^{i}_{PI} are number-average degree of polymerizations of polystyrene and polyisoprene block chains and given as $N^{i}_{PS} = M_n(PS)/104$, and $N^{i}_{PI} = M_n(PI)/68$, respectively. [b] $\bar{N}^{i}_{j}$ (j = PS or PI) is given by eq 29 in the text. [c] f_{PS} is defined as $f^{i}_{PS} = \bar{N}^{i}_{PS}/(\bar{N}^{i}_{PS} + \bar{N}^{i}_{PI})$, and corresponds to the volume fraction of PS-block in the ith (i = OSI-3 or H102) copolymer. [d] α_j (j = PS or PI) is given by eq 7 in the text. [e] p_j (j = PS or PI) is given by $p_j = A_j/a$, where A_j is the Kuhn statistical segment length of the jth polymer based on a common segment volume of a^3. Here we used $A_{PS} = 5.5$ Å and $A_{PI} = 6.0$ Å, respectively, based on a common segment volume of $a^3 = 1.08 \times 10^{-22}$ cm^3 in accordance with ref 51.

Table 4. Characteristics of the H102/OSI-3 Blends

H102/OSI-3 (wt %/wt %)	q_2 (mol fract of H102)	observed morphology
2/98	0.003	C[a]/L_s[b]
5/95	0.008	C/L_s
10/90	0.016	C/L_s
20/80	0.035	C/L_s
30/70	0.059	C/L_s
40/60	0.088	C/L_s
50/50	0.127	C/L_s
60/40	0.179	C
70/30	0.253	L_l[c]

[a] C denotes a PS-cylindrical morphology consisting of H102 and OSI-3. [b] L_s denotes lamellar microdomain morphology consisting of almost pure OSI-3. [c] L_l denotes single microdomain morphology of lamellae consisting of a large weight fraction of H102.

From Figure 7, parts a and b, we concluded the following: The SST formulation failed in predicting the PS cylinder morphology to become a stable morphology in H102/OSI-3 blend system, since in both parts a and b of Figure 7 the free energy curve of the PS cylinder is always higher than the lamellar morphology.[48] This unsuccess in predicting the stable morphology could be due to the inaccuracies in the SST and some degree of experimental error in the parameters. Nevertheless, it is clearly shown in Figure 7, parts a and b, that the free energy of the PS cylinder decreases more effectively than that of lamella when changing the blend composition from 70/30 to 60/40 or q_2 from 0.253 to 0.179. Therefore, the theory successfully predicted that blending of H102 and OSI-3 can lower the free energy of the cylindrical morphology very effectively at the experimentally relevant blend composition. The reason for this can be qualitatively explained as follows: In the SST, the free energy is expressed as the sum of contributions from the layer near to the interface that contains the smaller diblock (H_{A1} and H_{B1} in Figure 6) and the outer layer containing only the segments of the large copolymer (H_{A2} and H_{B2} in Figure 6). Since the grafting density of inner layer is much larger than that of outer layer (by a factor of $1/q_2$), the inner layer dominates the free energy. Therefore, an asymmetry of the smaller diblock (with its attendant spontaneous curvature) drives the system to cylinders, as opposed to lamellae. The small diblock does not form cylinders in its pure state because its spontaneous curvature is too small. The large diblock which is incorporated into the mixture produce a large radius of the cylinder, R. Therefore, the less the asymmetry of the smaller diblock the larger the large copolymer must be to allow formation of cylinders. The resulting cylinder must have the larger cylinder radius R. Unfortunately, increasing the size of the larger copolymer leads to macrophase separation before the formation of cylinders, which is unpredictable in the context of SST.

By comparing parts a and b of Figure 7, we found that the effect of conformational asymmetry between PS and PI segments makes the system more symmetric: The free energy difference between PS and PI cylinders was decreased and that between the PS cylinder and the lamella was increased. From eqs 18 and 20−22 we can find that ΔF_x (x denotes cylinder or lamella morphology) is a function of N^{1}_{B}/p_B and N^{1}_{A}/p_B, i.e., $\Delta F_x = \Delta F_x(N^{1}_{B}/p_B, N^{1}_{A}/p_B)$, and the symmetric condition can be attained when N^{1}_{A}/p_A is equal to N^{1}_{B}/p_B, i.e., $(N^{1}_{A}/p_A)(p_B/N^{1}_{B}) = 1$. In the case of H102/OSI-3 blend, the value of $(N^{OSI-3}_{PI}/p_{PI})(p_{PS}/N^{OSI-3}_{PS})$ is closer to unity than that of $N^{OSI-3}_{PI}/N^{OSI-3}_{PS}$, and therefore the system becomes more symmetric by taking the conformational asymmetry, i.e., $p_{PS} \neq p_{PI}$, into account. This tendency is consistent with the previous studies.[49]

B. Macrophase Separation between Constituent Copolymers in the Blend. In this section, we will briefly discuss about the macroscopic phase separation of the H102/OSI-3 blends. In this blend series, we observed the coexisting two phases for only the 20/80 blend. Further, the microdomain sizes and morphologies of these coexisting two phases turned out to be nearly identical to those observed in the 60/40 blend and 0/100 (i.e., OSI-3 neat) as mentioned above. Thus, we can speculate that, for the H102/OSI-3 blend, the miscibility limit of the weight fraction of OSI-3 is approximately 0.4 (see Figure 7). That is, (i) in the case where the weight fraction of OSI-3 is smaller than 0.4, H102 and OSI-3 are perfectly mixed and form a single microdomain structure, and (ii) in the case of the weight fraction of OSI-3 is larger than 0.4, some fraction of OSI-3 remains unmixed with H102 and forms its own microdomain structure.

Matsen[16] examined the miscibility of two symmetric AB-diblock copolymers with different polymerization indexes by using self-consistent field theory (SCFT). According to his prediction (cf. Figure 1 of ref 16), when the molecular weight ratio α, which is defined as $\alpha \equiv N_s/N_l$, where N_s and N_l are polymerization indices of short and long copolymers as a whole, respectively, is 0.15, the miscibility limit of the volume fraction of short diblock is 0.35 at $\chi N_l = 80$ or 0.40 at $\chi N_l = 200$ where χ is the Flory−Huggins interaction parameter between A and B segments. Note that for H102/OSI-3 blend, α is evaluated to be 0.15 and χN_l is evaluated to be between 100 and 200 where we have assumed χ to be given

$$\chi = 71.4/T - 0.0857 \qquad (30)$$

as reported by Rounds[50] and T is absolute temperature.

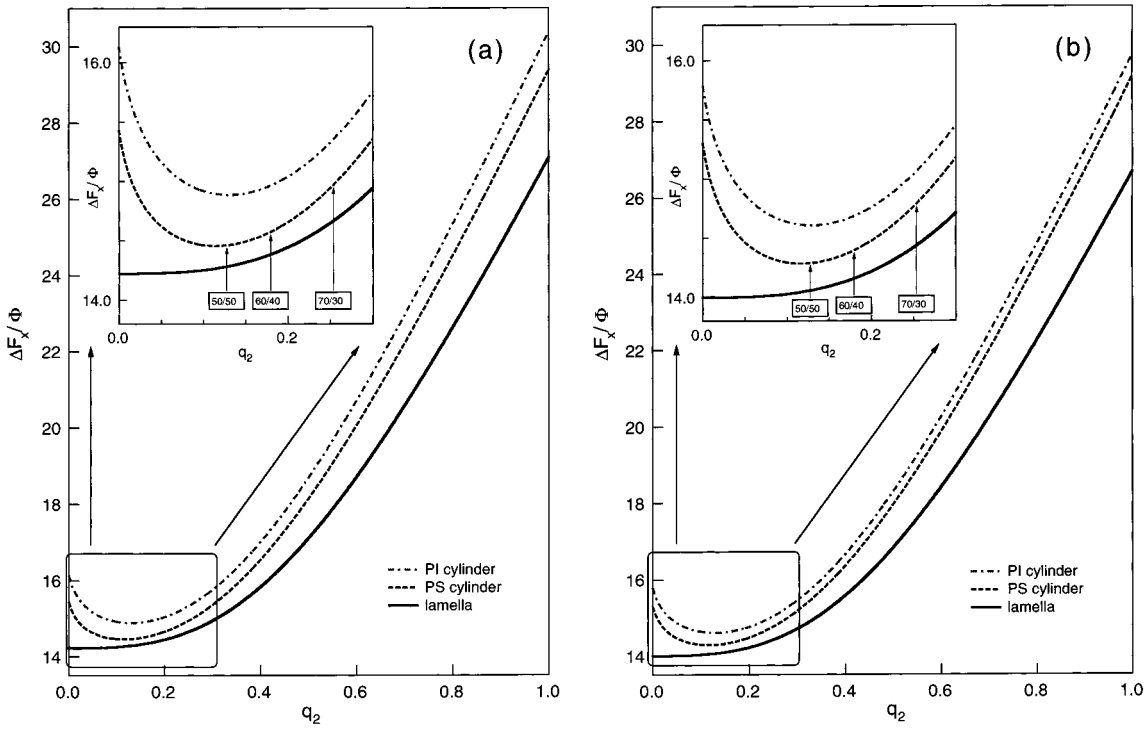

Figure 7. Results of model calculations for free energies of lamellar (solid lines) and PS−(dashed lines) or PI−(dash−dot lines) cylindrical morphology. The reduced free energy ($\Delta F_x/\Phi$) is plotted as a function of the number fraction of long diblock copolymer, q_2. In the calculation, the conformational asymmetry between PS and PI segments is not taken into account in part a, while it is taken into account in part b.

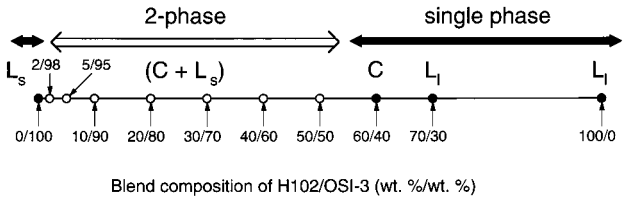

Figure 8. Phase diagram of the blends of the lamella-forming block copolymers OSI-3 and H102: (↔) the composition range where only the microphase separation occurs, resulting in the single microdomain morphology of the lamellae rich in the long block H102 (L_l), the PS-cylinder in the PI matrix (C), and the lamellae rich in the short block OSI-3 (L_s); (⇔) the composition range where the macrophase separation occurs resulting in the phase composed of C and the phase composed of L_s.

Thus, our experimental result is consistent with the SCFT theory[16] with respect to the miscibility behavior.

V. Concluding Comments

A partially miscible pair of nearly symmetric polystyrene (PS)-*block*-polyisoprene (PI) copolymers having different total molecular weights was investigated using small-angle X-ray scattering and transmission electron microscopy. This blend system showed the following behavior with increasing the weight fraction of the short diblock copolymer: first the domain size or periodicity decreased with maintaining lamellar morphology until the weight fraction of short diblock reached to 0.3, then the morphology transition from lamella to PS cylinder occurred when the weight fraction of short diblock was 0.4, and a macrophase separation into the phase composed of PS cylinder and the phase composed of short diblock copolymer appeared in the specimen when the weight fraction of short diblock exceeded 0.4 (which is schematically summarized in Figure 8). These behaviors were compared with theoretical works of strong segregation theory and self-consistent field theory, and reasonably good agreements were obtained. It turned out to be clear from this study that for blends of nearly symmetric diblock copolymers, the slight asymmetry in composition of each block copolymer is well enhanced and reflected in their morphologies.

Acknowledgment. We would like to thank Professor Tatiana M. Birshtein for very useful suggestions. We would like to thank also Dr. François Court for useful discussions.

References and Notes

(1) Hashimoto, T. in *Thermoplastic Elastomers, A Comprehensive Review*; Legge, N. R., Holden, G., Schroeder, H. E., Ed.; Hanser: Munich, Germany, 1996; p 429. Hasegawa, H.; Hashimoto, T. In *Comprehensive Polymer Science, Second Supplement*; Aggarwal, S. L., Russo, S., Vol. Eds.; Pergamon: Oxford, England, 1996; pp 497.
(2) Bates, F. S.; Fredrickson, G. H. *Annu. Rev. Phys. Chem.* **1990**, *41*, 525.
(3) Hadziioannou, G.; Skoulios, A. *Macromolecules* **1982**, *15*, 267.
(4) Hashimoto, T. *Macromolecules* **1982**, *15*, 1548.
(5) Hashimoto, T.; Yamasaki, K.; Koizumi, S.; Hasegawa, H. *Macromolecules* **1993**, *26*, 2895.
(6) Hashimoto, T.; Koizumi, S.; Hasegawa, H. *Macromolecules* **1994**, *27*, 1562.
(7) Koizumi, S.; Hasegawa, H.; Hashimoto, T. *Macromolecules* **1994**, *27*, 4371.
(8) Court, F. These de Doctorat de l'Université Pierre et Marie Curie, 1996.
(9) Spontak, R. J.; Fung, J.; C.; Braunfeld, M. B.; Sedat, J. W.; Agard, D. A.; Kane, L.; Smith, S. D.; Satkowski, M. M.; Ashraf, A.; Hajduk, D. A.; Gruner, S. M. *Macromolecules* **1996**, *29*, 4494.
(10) Yamaguchi, D.; Hashimoto, T.; Han, C. D.; Baek, D. M.; Kim, J. K.; Shi, A.-C. *Macromolecules* **1997**, *30*, 5832.
(11) Yamaguchi, D.; Bodycomb, J.; Koizumi, S.; Hashimoto, T. *Macromolecules* **1999**, *32*, 5844.

(12) Milner, S. T.; Witten, T. A.; Cates, M. E. *Macromolecules* **1989**, *22*, 853.
(13) Birshtein, T. M.; Liatskaya, Yu. V.; Zhulina, E. B. *Polymer* **1990**, *31*, 2185.
(14) Shi, A.-C.; Noolandi, J. *Macromolecules* **1994**, *27*, 2936.
(15) Shi, A.-C.; Noolandi, J. *Macromolecules* **1995**, *28*, 3103.
(16) Matsen, M. W. *J. Chem. Phys.* **1995**, *103*, 3268.
(17) Matsen, M. W.; Bates, F. S. *Macromolecules* **1995**, *28*, 7298.
(18) Hashimoto, T.; Shibayama, M.; Kawai, H. *Macromolecules* **1983**, *16*, 1093.
(19) Kane, L.; Satkowski, M. M.; Smith, S. D.; Spontak, R. J. *Macromolecules* **1996**, *29*, 8862.
(20) Lin, E. K.; Gast, A. P.; Shi, A.-C.; Noolandi, J.; Smith, S. D. *Macromolecules* **1996**, *29*, 5920.
(21) Papadakis, C. M.; Mortensen, K.; Posselt, D. *Eur. Phys. J. B* **1998**, *4*, 325.
(22) Almdal, K.; Rosedale, J. H.; Bates, F. S. *Macromolecules* **1990**, *23*, 4336.
(23) Lyatskaya, Ju. V.; Zhulina, E. B.; Birshtein, T. M. *Polymer* **1992**, *33*, 343.
(24) Zhulina, E. B.; Birshtein, T. M. *Polymer* **1991**, *32*, 1299.
(25) (a) Koizumi, S.; Hasegawa, H.; Hashimoto, T. *Macromolecules* **1994**, *27*, 6532. (b) Koizumi, S.; Hasegawa, H.; Hashimoto, T. *Macromolecules* **1994**, *27*, 7893.
(26) Sakamoto, N.; Hashimoto, T. *Macromolecules* **1995**, *28*, 6825.
(27) Hashimoto, T.; Suehiro, S.; Shibayama, M.; Saijo, K.; Kawai, H. *Polym. J.* **1981**, *13*, 501.
(28) Suehiro, S.; Saijo, K.; Ohta, Y.; Hashimoto, T. *Anal. Chim. Acta* **1986**, *189*, 41.
(29) Fujimura, M.; Hashimoto, T.; Kawai, H. *Mem. Fac. Eng., Kyoto University* **1981**, *43* (2), 224.
(30) Hasegawa, H.; Tanaka, H.; Yamasaki, K.; Hashimoto, T. *Macromolecules* **1987**, *20*, 1651.
(31) Shibayama, M.; Hashimoto, T. *Macromolecules* **1986**, *19*, 740.
(32) Hashimoto, T.; Nagatoshi, K.; Todo, A.; Hasegawa, H.; Kawai, H. *Macromolecules* **1974**, *7*, 364.
(33) Hashimoto, T.; Fujimura, M.; Kawai, H. *Macromolecules* **1980**, *13*, 1660.
(34) Hosemann, R.; Bagachi, S. N. *Direct Analysis of Diffraction by Matter*; North-Holland: Amsterdam, 1962.
(35) Kimishima, K.; Jinnai, H.; Hashimoto, T. *Macromolecules* **1999**, *32*, 2585.
(36) Hashimoto, T.; Kawamura, T.; Harada, M.; Tanaka, H. *Macromolecules* **1994**, *27*, 3063.
(37) Sakamoto, N.; Hashimoto, T. *Macromolecules* **1998**, *31*, 3815.
(38) Hong, S.-U.; Laurer, J. H.; Zielinski, J. M.; Samseth, J.; Smith, S. D.; Duda, J. L.; Spontak, R. J. *Macromolecules* **1998**, *31*, 2174.
(39) Zhulina, E. B.; Lyatskaya, Y. V.; Birshtein, T. M. *Polymer* **1992**, *33*, 332.
(40) Birshtein, T. M.; Lyatskaya, Y. V.; Zhulina, E. B. *Polymer* **1992**, *33*, 2750.
(41) Flory, P. J. *Principles of Polymer Chemistry*; Cornell University Press: Ithaca, NY, 1953; pp 402, 427. Volkenstein, M. V. *Configurational Statistics of Polymeric Chains*; Interscience: New York, 1963; p 257. Hill, T. *Introduction to Statistical Thermodynamics*; Addison-Wesley: Reading, MA, 1960; Chapter 13. Treloar, L. R. G. *The Physics of Rubber Elasticity*, 2nd ed.; Oxford: Oxford, England, 1958; Chapter III.
(42) Hashimoto, T.; Shibayama, M.; Kawai, H. *Macromolecules* **1980**, *13*, 1237.
(43) Birshtein, T. M. Private communications.
(44) Sakurai, S.; Mori, K.; Okawara, A.; Kimishima, K.; Hashimoto, T. *Macromolecules* **1992**, *25*, 2679.
(45) Fetters, L. J.; Lohse, D. J.; Richter, D.; Witten, T. A.; Zirkel, A. *Macromolecules* **1994**, *27*, 4639.
(46) Sakurai, S.; Irie, H.; Umeda, H.; Nomura, S.; Lee, H. H.; Kim, J. K. *Macromolecules* **1998**, *31*, 336.
(47) Bates, F. S.; Fredrickson, G. H. *Macromolecules* **1994**, *27*, 1065.
(48) We would like to note that when we used the values of N_j^i (j = PS or PI and i = OSI-3 or H102) in Table 3 instead of those of $\overline{N_j^i}$ and we did not take conformational asymmetry between PS and PI segments into account in the calculation, there were intersections between the free energy curves of lamella and PS cylinder so that the cylinder phase has a lower free energy than the lamellar phase, and SST successfully predicted our experimental result, although the calculation, which does not take the correction for the monomer volume difference into account, might not be proper.
(49) Bates, F. S.; Schulz, M. F.; Khandpur, A. K.; Förster, S.; Rosedale, J. H.; Almdal, K.; Mortensen, K. *Faraday Discuss.* **1994**, *98*, 7. Birshtein, T. M.; Lyatskaya, Y. V. *Polym. Sci. Russ., Ser. A* **1995**, *37*, 154.
(50) Rounds, N. A.; Ph.D. Dissertation, University of Akron, 1970.
(51) Gehlsen, M. D.; Bates, F. S. *Macromolecules* **1993**, *26*, 4122. Bandrup, J., Immergut, E. H., Eds. *Polymer Handbook*; Wiley: New York, 1975.

MA000827D